Journal of Modeling and Simulation of Microsystems, Vol. 1, No. 2, Pages 139-148, 1999.

A MODEL OF PHOTOELECTRIC PHENOMENA IN MOS STRUCTURES AT LOW ELECTRIC FIELDS

H.M. Przewlocki†
Institute of Electron Technology, 02-668 Warsaw, Poland.

Abstract

A comprehensive model is presented of the internal photoemission in MOS systems, at low electric fields ($|\mathscr{E}| < 10^4\ V/cm$) in the dielectric. Model equations are separately solved for the case of zero photocurrent ($J = 0$) and for nonzero photocurrent ($J \neq 0$), allowing calculation of various photoelectric characteristics of MOS structures. These calculated characteristics are shown to remain in excellent agreement with the experimental ones, taken for a range of different MOS structures, which strongly supports the validity of the model. It is also shown that based on this model new, highly precise MOS structure photoelectric measurement methods can be developed.

Keywords: semiconductors, dielectrics, MOS structure, photoelectric phenomena, internal photoemission

1. Introduction

Internal photoemission characteristics of the metal-oxide-semiconductor (MOS) system have been, for many years, used to determine basic physical parameters of MOS structures (see [1,2]). Experimentally taken characteristics, such as photocurrent vs. gate voltage, $I(V_G)$, or photocurrent vs. wavelength, $I(\lambda)$ characteristics of these structures have been interpreted using the physical model, developed in the seventies by Powell and Berglund [3-5]. This model is based on the assumption, that photocurrent is limited by the number of carriers passing into the dielectric, over the potential barrier at the emitter-dielectric interface. Hence, this model applies when electric field in the dielectric, $\mathscr{E}$, is strong enough to move essentially all the carriers photoinjected into the dielectric to the other electrode of the MOS system. Roughly speaking, such a situation sets in for $|\mathscr{E}| > 10^5\ V/cm$.

It was however shown recently, that very useful information about some of the basic MOS system parameters can be obtained from photoelectric characteristics taken in the range of very low electric fields in the dielectric ($|\mathscr{E}| < 10^4\ V/cm$) [6-10]. Hence, a model was needed which would allow interpretation of MOS system internal photoemission characteristics taken in the range of weak electric fields in the dielectric. Such a model has been developed, experimentally verified and applied to develop new, photoelectric MOS system measurement methods [8-11].

In this article the main features of the model are outlined and calculations based on this model are discussed and compared with experimentally taken photoelectric characteristics of various MOS structures.

†hmp@ite.waw.pl

2. Theory

2.1. Formulation of the problem

A setup is considered, in which the MOS structure, with a semitransparent gate, is uniformly illuminated by UV radiation of wavelength λ, as shown in Fig. 1. The gate voltage V_G is applied and the photocurrent I is measured in the external circuit. The wavelength λ is varied over the range of values at which photoinjection of electrons from both the gate and the substrate into conduction band of the oxide takes place. The gate voltage V_G is varied over the range of values for which the electric field $\mathscr{E}$ in the dielectric remains small.

The setup shown in Fig. 1 allows accurate measurement of photocurrent-gate voltage $I(V_G)$ characteristics, for different wavelengths λ of UV radiation, as well as, very accurate determination of the V_G^0 voltage, at which the photocurrent I changes sign ($I = 0$), for a given wavelength λ. Both these characteristics (i.e. $I(V_G)$ and $V_G^0(\lambda)$) will be used in experimental verification of the model.

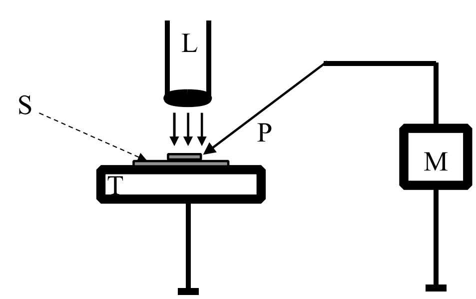

Fig. 1: Schematic illustration of the setup considered. S - MOS structure with semitransparent gate, L - UV illumination system, P - contact probe, M - voltage source and current measurement unit, T – measurement stage.

In the formulation of the problem, the following assumptions are made:

- The photocurrent I is entirely due to electrons photoinjected into the conduction band of the oxide (photoinjection of holes is negligible).
- Tunneling and leakage currents are negligible.
- A considerable space charge exists in the oxide, due to large fluxes of electrons photoinjected from both the gate and the substrate and to the weak electric field $\mathcal{E}$.
- This space charge consists of free electrons (electrons in the conduction band of the oxide, which take part in conducting current) and electrons trapped in trapping centers, which are uniformly distributed in the oxide. At any position in the dielectric, a fixed fraction θ of the total charge density resides in the conduction band, while the remaining electrons are trapped.
- The problem may be considered as one dimensional.

With these assumptions, the current I measured in the external circuit should be considered as space charge limited current in the oxide and since weak electric field exists there, the diffusion component of this current has to be taken into account.

Hence, the problem is fully described by the following equations

- The current flow equation:

$$j = q\mu n_c(x)\mathcal{E}(x) + \mu kT\frac{dn_c}{dx} \tag{1}$$

in which j is current density, q electron charge, μ electron mobility in the oxide, n_c free electron density in the oxide, $\mathcal{E}$ electric field in the oxide, x is a coordinate perpendicular to gate-oxide and oxide-semiconductor interfaces ($x = 0$ at gate-oxide interface), k is Boltzmann's constant and T is temperature;

- The Poisson equation:

$$\frac{d\mathcal{E}}{dx} = -\frac{qn(x)}{\epsilon} \tag{2}$$

in which n is total density of electrons, i.e., the sum of free electron density n_c and trapped electron density n_T, and ϵ is electric permittivity of the oxide.

- The relation between free (n_c) and total (n) electron densities:

$$n_c = \theta \cdot n \tag{3}$$

where θ is constant.

To solve these three equations, following dimensionless variables are introduced:

- distance

$$z = \frac{x}{t_I} \tag{4a}$$

where t_I is oxide thickness;

- potential

$$\phi = \frac{qV}{kT} \tag{4b}$$

where V is potential in the oxide;

- electric field

$$E = \mathcal{E}\frac{qt_I}{kT} = -\frac{d\phi}{dz} \tag{4c}$$

- current density

$$J = j\frac{q^2t_I^3}{\epsilon\mu k^2T^2\theta} \tag{4d}$$

- electron density

$$N = n\frac{q^2t_I^2}{\epsilon kT} \tag{4e}$$

Using these dimensionless variables and combining Eqs. (1)-(3), a third order differential equation is obtained:

$$J = \frac{d^3\phi}{dz^3} - \frac{d^2\phi}{dz^2}\frac{d\phi}{dz} \tag{5}$$

which should be solved, subject to boundary conditions, resulting from normalized Eq. (2):

$$\frac{d^2\phi}{dz^2}(z = 0) = N(0) \tag{6a}$$

$$\frac{d^2\phi}{dz^2}(z = 1) = N(1) \tag{6b}$$

where $N(0)$ and $N(1)$ are dimensionless electron densities at $z = 0$ and $z = 1$.

Eq. (5) can be immediately integrated once, yielding:

$$Jz + C_1 = \frac{d^2\phi}{dz^2} - \frac{1}{2}\left(\frac{d\phi}{dz}\right)^2 \tag{7}$$

where C_1 is the first constant of integration. Substituting into Eq. (7):

$$\phi = -2\ln y \tag{8}$$

one obtains the equation

$$\frac{d^2y}{dz^2} + \frac{1}{2}(Jz + C_1)y = 0 \tag{9}$$

which will be further called the transitional equation.

The transitional equation will now be separately solved for $J = 0$ and for $J \neq 0$.

2.2. Solution of the problem for J = 0

In this case the straightforward solution of Eq. (9) is:

$$y = C_2\sin\omega z + C_3\cos\omega z \tag{10}$$

with:

$$\omega = \pm\sqrt{\frac{C_1}{2}} \tag{11}$$

and with C_2, C_3 being constants of integration.

Since C_1 can be either positive or negative (or zero), the value of ω is either real or imaginary, as results from Eq. (11). Both these cases will be considered now.

2.2.1. Case 1: ω is real

It results from Eqs. (8),(10) that:

$$\phi(z) = -2\ln[C_2 \sin \omega z + C_3 \cos \omega z] \tag{12}$$

Assuming that†:

$$\phi(z = 1) = 0 \tag{13}$$

one gets:

$$C_2 \sin \omega + C_3 \cos \omega = 1 \tag{14}$$

The values of C_2 and C_3 can be found making use of the boundary conditions (6). Hence Eq. (12) is differentiated twice, to give:

$$N(z) = 2\omega^2 \frac{C_2^2 + C_3^2}{(C_2 \sin \omega z + C_3 \cos \omega z)^2} \tag{15}$$

which for $z = 0$, is:

$$N(0) = 2\omega^2 \frac{C_2^2 + C_3^2}{C_3^2} \tag{16}$$

and for $z = 1$, is:

$$N(1) = 2\omega^2 \frac{C_2^2 + C_3^2}{(C_2 \sin \omega + C_3 \cos \omega)^2} \tag{17}$$

Taking Eq. (14) into account, one obtains from Eqs. (16),(17):

$$C_2 = \frac{1}{r}\sqrt{\frac{N(0) - 2\omega^2}{2\omega^2}} \tag{18a}$$

$$C_3 = \frac{1}{r} \tag{18b}$$

Here, r is defined as:

$$r \equiv \sqrt{\frac{N(0)}{N(1)}} \tag{19}$$

Using these results in Eq. (12), one obtains:

$$\phi(z) = -2\ln\left\{\frac{1}{r}\left[\sqrt{\frac{N(0) - 2\omega^2}{2\omega^2}} \sin \omega z + \cos \omega z\right]\right\} \tag{20}$$

†This assumption is different from the one made in [9].

$$E(z) = -\frac{d\phi}{dz} = 2\omega \frac{\sqrt{\frac{N(0) - 2\omega^2}{2\omega^2}} \cos \omega z - \sin \omega z}{\sqrt{\frac{N(0) - 2\omega^2}{2\omega^2}} \sin \omega z + \cos \omega z} \tag{21}$$

$$N(z) = \frac{d^2\phi}{dz^2} = \frac{N(0)}{\left(\sqrt{\frac{N(0) - 2\omega^2}{2\omega^2}} \sin \omega z + \cos \omega z\right)^2} \tag{22}$$

Using $z = 1$ in Eq. (22), one gets the following equation:

$$N(0)(\sin \omega)^2 = 2\omega^2(1 + r^2 - 2r\cos \omega) \tag{23}$$

which can be used to find the value of ω for given values of $N(0)$ and $N(1)$.

Eqs. (20)-(23) allow calculation of dimensionless potential ϕ, dimensionless electric field E and dimensionless electron density N distributions in the dielectric of the MOS system, for known values of dimensionless electron densities $N(0)$ and $N(1)$, at both interfaces of this dielectric.

2.2.2. Case 2: ω is imaginary

In this case:

$$\omega = i\omega_1 \tag{24}$$

and use is made of the following well known relations:

$$\cos ix = \cosh x \tag{25a}$$

$$\sin ix = i \sinh x \tag{25b}$$

Inserting Eqs. (24) and (25) into Eqs. (20)-(23) one obtains:

$$\phi(z) = -2\ln\left\{\frac{1}{r}\left[\cosh \omega_1 z - \sqrt{\frac{N(0) + 2\omega_1^2}{2\omega_1^2}} \sinh \omega_1 z\right]\right\} \tag{26}$$

$$E(z) = 2\omega_1 \frac{\sinh \omega_1 z - \sqrt{\frac{N(0) + 2\omega_1^2}{2\omega_1^2}} \cosh \omega_1 z}{\cosh \omega_1 z - \sqrt{\frac{N(0) + 2\omega_1^2}{2\omega_1^2}} \sinh \omega_1 z} \tag{27}$$

$$N(z) = \frac{N(0)}{\left(\cosh \omega_1 z - \sqrt{\frac{N(0) + 2\omega_1^2}{2\omega_1^2}} \sinh \omega_1 z\right)^2} \tag{28}$$

and:

$$N(0)(\sinh \omega_1)^2 = 2\omega_1^2(1 + r^2 - 2r\cosh \omega_1) \tag{29}$$

In case of imaginary values of ω, Eqs. (26)-(29) serve the same purposes as Eqs. (20)-(23), in case of real values of ω.

Examples of $\phi(z)$, $E(z)$ and $N(z)$ distributions calculated using Eqs. (20)-(23) and Eqs. (26)-(29), for $N(1)=1$ and for different $N(0)$ values are shown in Fig. 2.

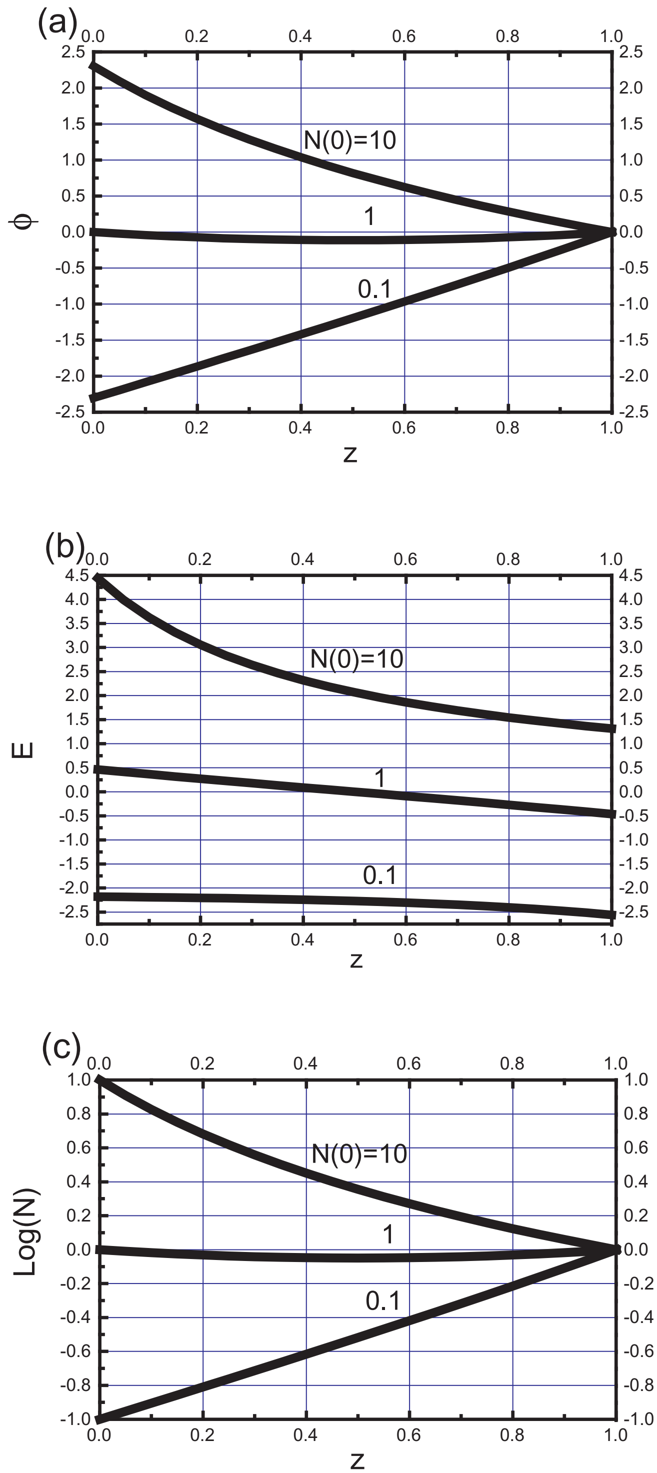

Fig. 2: Distribution of the (a) dimensionless potential ϕ(z), (b) dimensionless electric field $E(z)$ and (c) logarithm of dimensionless electron density $N(z)$ in the dielectric, calculated using Eqs. (20)-(23) and (26)-(29) for $N(1) = 1$ and $N(0) = 0.1$, 1 and 10.

For practical applications of this model it is particularly important to know the value of the total voltage drop in the dielectric V_I^0, which corresponds with $J = 0$.

With the assumption expressed by Eq. (13), the total dimensionless voltage drop in the dielectric is equal $\phi(0)$. From both, Eqs. (20),(26), it results that:

$$\phi(0) = \ln\frac{N(0)}{N(1)} \tag{30}$$

Hence, using Eq. (4b):

$$V_I^0 = \frac{kT}{q}\ln\frac{N(0)}{N(1)} \tag{31}$$

The values of $N(0)$ and $N(1)$ depend on the densities of electron fluxes photoinjected from the gate and from the substrate into the dielectric, hence it is assumed that:

$$\frac{N(0)}{N(1)} = \left|\frac{j_G}{j_S}\right| \tag{32}$$

where j_G, j_S are current densities injected from the gate and from the substrate. According to [3-5], these current densities can be expressed as:

$$j_G = a_G(\lambda)(h\nu - E_{BG})^{p_G} \tag{33a}$$

$$j_S = a_S(\lambda)(h\nu - E_{BS})^{p_S} \tag{33b}$$

where $h\nu$ is photon energy, E_{BG}, E_{BS} are barrier heights for photoinjection at gate-dielectric and substrate-dielectric interfaces, p_G, p_S are exponents dependent on the type of the emitter and $a_G(\lambda)$, $a_S(\lambda)$ are functions of λ which are characteristic for gate-dielectric and substrate-dielectric interfaces. These a(λ) functions are approximated here by the product:

$$a(\lambda) = F(\lambda)G(\lambda)H \tag{34}$$

where $F(\lambda)$ is a function representing the dependence of UV radiation energy on the wavelength λ (which may be a characteristic of the UV illumination system used), $G(\lambda)$ is the fraction of UV radiation energy absorbed by the emitter (gate or substrate) and H is assumed to be a constant, independent of λ.

For injection from the gate $G(\lambda) = A(\lambda)$, where $A(\lambda)$ is the fraction of UV radiation energy absorbed by the gate. For injection from the substrate $G(\lambda) = T(\lambda)$, where $T(\lambda)$ is the fraction of UV radiation energy transmitted to (and absorbed by) the substrate, as discussed in detail in [12,13].

From Eqs. (32)-(34) it results that:

$$\frac{N(0)}{N(1)} = R\frac{A(\lambda)}{T(\lambda)}\frac{(h\nu - E_{BG})^{p_G}}{(h\nu - E_{BS})^{p_S}} \tag{35}$$

where R is a constant. Using Eqs. (31) and (35) one obtains:

$$V_I^0 = \frac{kT}{q}\left[\ln\frac{A(\lambda)}{T(\lambda)} + \ln\frac{(h\nu - E_{BG})^{p_G}}{(h\nu - E_{BS})^{p_S}} + \ln R\right] \tag{36}$$

Eq. (36) describes the dependence of the V_I^0 value on the wavelength λ. In practice however, it is the gate voltage V_G^0 (i.e. the gate voltage at which $J = 0$), which can be measured (not the V_I^0 value). Hence, the relation between V_G^0 and V_I^0 has to be found.

In general, the gate voltage V_G is given by the sum [1,2]:

$$V_G = V_I + V_S + \phi_{MS} \tag{37}$$

where V_I is the voltage drop in the dielectric V_S is semiconductor surface potential and ϕ_{MS} is the effective contact potential difference between the gate and the substrate.

In case of $J = 0$, Eq. (37) becomes:

$$V_G^0 = V_I^0 + V_S^0 + \phi_{MS} \tag{38}$$

where V_G^0, V_I^0 and V_S^0 are the V_G, V_I and V_S values at $J = 0$.

Combining Eqs. (36),(38) yields:

$$V_G^0 = \frac{kT}{q}\left[\ln\frac{A(\lambda)}{T(\lambda)} + \ln\frac{(h\nu - E_{BG})^{p_G}}{(h\nu - E_{BS})^{p_S}}\right] + C \tag{39}$$

where:

$$C = \frac{kT}{q}\ln R + V_S^0 + \phi_{MS} \tag{40}$$

For certain MOS structures (e.g. for structures with heavily doped substrates, for which the dependence of V_S^0 on λ is negligible), the value of C becomes a constant. For such structures Eq. (39) allows calculation of $V_G^0 = f(\lambda)$ characteristics, with the accuracy to the constant C. The $A(\lambda)$ and $T(\lambda)$ functions can be determined from purely optical considerations, such as the ones applied in [13], using the values of optical indexes published in literature [14-16]. Such theoretical characteristics of Al-SiO_2-Si structures, calculated for different oxide thicknesses t_I are shown in Fig. 3. For calculation of these curves, following values of the parameters were used: $E_{BG} = 3.4$ *eV*, $E_{BS} = 4.35$ *eV*, $p_G = 3$, $p_S = 3$.

As can be seen in Fig. 3, the shapes of $V_G^0 = f(\lambda)$ characteristics change dramatically with changing the oxide thickness t_I, which demonstrates the importance of optical phenomena (optical interference in the system) in MOS structures, for their photoelectric characteristics. This property will be used in section 3, for experimental verification of the above considerations.

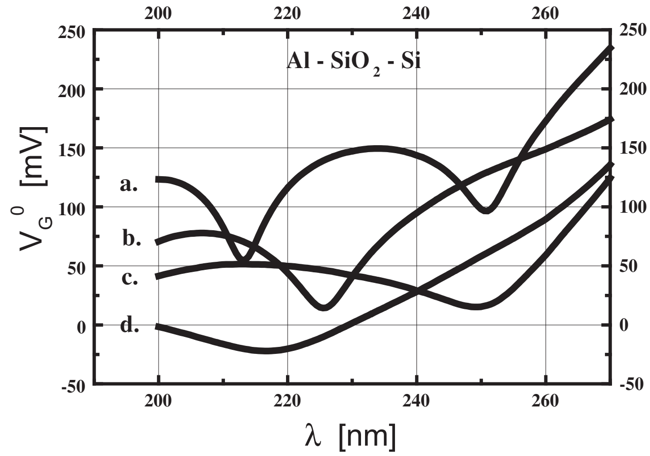

Fig. 3: The $V_G^0 = f(\lambda)$ curves calculated using eq. (39) for the Al-SiO_2_Si system with different thicknesses t_I of the SiO_2 layer. Values of the constant C have been arbitrarily chosen for each curve, so as to better demonstrate differences in shapes of the curves. Curve a: t_I = 400 *nm*, C = 80 *mV*; curve b: t_I = 280 *nm*, C = 30 *mV*; curve c: t_I = 150 *nm*, C = 0; curve d: t_I = 55 *nm*, C = 0.

It should also be noticed, that as results from Eq. (31) the voltage drop in the dielectric V_I^0 is equal zero for $N(0) = N(1)$. The corresponding gate voltage is denoted V_{G0} and this state of the MOS structure is called zero dielectric voltage (ZDV). Hence, for $N(0) = N(1)$, $V_I^0 = 0$, $V_G^0 = V_{G0}$ and the MOS system reaches the ZDV state. Photoelectric characteristics can be used for accurate determination of the V_{GO} value, as discussed further in the next subsection.

2.3. Solution of the problem for $J \neq 0$

For $J \neq 0$, Eq. (9) belongs to the class of Bessel type equations and mathematically similar problems have usually been solved in terms of Bessel and/or modified Bessel functions [17-19]. In this article a different approach will be applied and a simpler solution will be found in terms of Airy functions [11].

Lets define a parameter u:

$$u = -(2J^2)^{-1/3}(Jz + C_1)\,[\tag{41}$$

Substitution of this parameter into the transitional Eq. (9), yields the Airy equation [20,21]:

$$\frac{d^2y}{du^2} - uy = 0 \tag{42}$$

with the solution:

$$y = A[Ai(u) + C_4 Bi(u)] \tag{43}$$

where $Ai(u)$ and $Bi(u)$ are the first and the second Airy functions of the parameter u, while A and C_4 are constants of integration.

Denoting:

$$u = u_0 \qquad \text{for} \qquad z = 0 \tag{44a}$$

$$u = u_1 \qquad \text{for} \qquad z = 1 \tag{44b}$$

and using Eqs. (44) in Eq. (41), one finds:

$$J = 2(u_0 - u_1)^3 \tag{45}$$

and:

$$C_1 = -2u_0(u_0 - u_1)^2 \tag{46}$$

The dimensionless voltage drop in the dielectric $\Delta\phi$ is given by:

$$\Delta\phi = \phi(0) - \phi(1) \tag{47}$$

which using eqs. (8) and (43), yields:

$$\Delta\phi = 2\ln\frac{Ai(u_1) + C_4Bi(u_1)}{Ai(u_0) + C_4Bi(u_0)} \tag{48}$$

To find the value of C_4, boundary conditions (6) are used again.

For that purpose, second derivative of the potential $\frac{d^2\phi}{dz^2}$ has to be found. Making use of Eqs. (8), (9), (41) and (43), one finds [11]:

$$\frac{d^2\phi}{dz^2} = u(2J^2)^{1/3}\left\{\frac{1}{u}\left[\frac{Ai'(u) + C_4Bi'(u)}{Ai(u) + C_4Bi(u)}\right]^2 - 1\right\} \tag{49}$$

where $Ai'(u)$ and $Bi'(u)$ are the third and the fourth Airy functions of the parameter u ($Ai'(u) = \frac{d}{du}[Ai(u)]$; $Bi'(u) = \frac{d}{du}[Bi(u)]$).

For $z = 0$ one obtains:

$$N(0) = u_0(2J^2)^{1/3}\left\{\frac{1}{u_0}\left[\frac{Ai'(u_0) + C_4Bi'(u_0)}{Ai(u_0) + C_4Bi(u_0)}\right]^2 - 1\right\} \tag{50}$$

and for $z = 1$ one gets:

$$N(1) = u_1(2J^2)^{1/3}\left\{\frac{1}{u_1}\left[\frac{Ai'(u_1) + C_4Bi'(u_1)}{Ai(u_1) + C_4Bi(u_1)}\right]^2 - 1\right\} \tag{51}$$

Finding out the value of C_4, from both (50) and (51), yields [11]:

$$C_4 = -\frac{Ai'(u_0) - k_0Ai(u_0)}{Bi'(u_0) - k_0Bi(u_0)} \tag{52}$$

and

$$C_4 = -\frac{Ai'(u_1) - k_1Ai(u_1)}{Bi'(u_1) - k_1Bi(u_1)} \tag{53}$$

where k_0 and k_1 have been defined as:

$$k_0 = \pm\frac{\sqrt{N(0) + 2u_0(u_0 - u_1)^2}}{\sqrt{2}(u_0 - u_1)} \tag{54}$$

$$k_1 = \pm\frac{\sqrt{N(1) + 2u_1(u_0 - u_1)^2}}{\sqrt{2}(u_0 - u_1)} \tag{55}$$

Eliminating C_4 from Eqs. (52) and (53), yields:

$$\begin{aligned} &Ai'(u_0)Bi'(u_1) - k_0Ai(u_0)Bi'(u_1) - \\ &k_1Ai'(u_0)Bi(u_1) + k_0k_1Ai(u_0)Bi(u_1) = \\ = \;&Bi'(u_0)Ai'(u_1) - k_0Bi(u_0)Ai'(u_1) - \\ &k_1Bi'(u_0)Ai(u_1) + k_0k_1Bi(u_0)Ai(u_1) \end{aligned} \tag{56}$$

Eq. (56) determines the relation that exists between the values of u_0 and u_1, for given values of $N(0)$ and $N(1)$. Hence, for given $N(0)$ and $N(1)$ and for a given or assumed value of u_0 (or u_1), the corresponding value of u_1 (or u_0) can be found by solving Eq. (56).

Having found the pairs of corresponding u_0 and u_1 values, all the quantities which are needed to determine photoelectric characteristics of the MOS system can be found using Eqs. (45)-(48) and (52)-(55). This way, the dimensionless photocurrent J vs. dimensionless voltage drop in the dielectric $\Delta\phi$ characteristics can be calculated, for different values of the wavelength λ.

It is important to notice here, that the dimensionless current-voltage ($J = f(\Delta\phi)$) characteristics become symmetrical with respect to the $J = 0$ point, i.e.:

$$J(\Delta\phi) = -J(-\Delta\phi) \tag{57}$$

when

$$N(0) = N(1) \tag{58}$$

since in this case the the exchange of values between $N(0)$ and $N(1)$ does not change the boundary conditions (see Eqs, (6)). This property is very useful in determining, which one of a set of $J = f(\Delta\phi)$ characteristics, taken for different wavelengths λ, corresponds with the $N(0) = N(1)$ condition, thus, in determining the V_{GO} voltage, as described in the next section.

3. Experimental Verification

Theoretical considerations presented above have been experimentally verified and the verification results will be demonstrated now, both for the case of $J = 0$ and for the case of $J \neq 0$.

3.1. Verification for the case of J = 0

In this case, use is made of the fact that the shape of the $V_{G0} = f(\lambda)$ characteristic strongly depends on the thickness of the dielectric layer, as shown in Fig. 3. Hence, a series of such characteristics was taken for Al-SiO_2-Si(N^+) and Al-SiO_2-Si(P^+) structures with different thicknesses t_I of the SiO_2 layer. The measured structures had the same thickness of the Al gate and their SiO_2 layer thickness t_I varied in the range t_I = (50 - 400) *nm*.

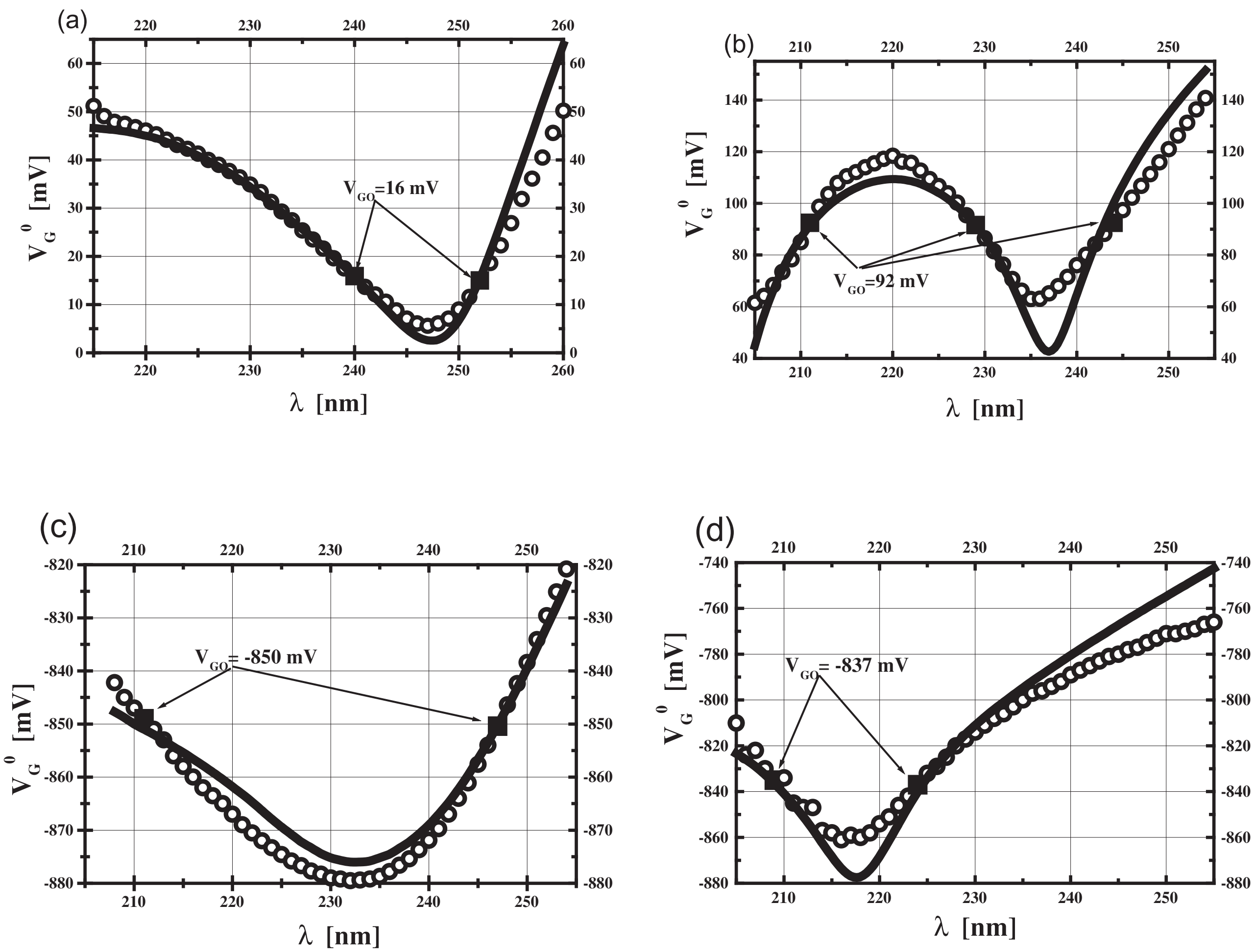

Fig. 4: Comparison of experimental $V_G^0 = f(\lambda)$ characteristics (circles) with theoretical curves (solid lines) calculated using eq. (39) for Al-SiO_2-Si (N^+) and Al-SiO_2-Si(P^+) structures with various thicknesses t_I of SiO_2 layers. (a), (b) are for N^+ substrate and (c), (d) are for P^+ substrate structures. Below, t_I and C values are given, which were used in calculations of theoretical curves to obtain best fit between theory and experiment. Values of V_{GO} are marked by solid squares. (a) t_I = 306 *nm*, C = 70 *mV*; (b) t_I = 375 *nm*, C = 50 *mV*; (c) t_I = 62 *nm*, C = -872 *mV*; (d) t_I = 196 *nm*, C = -855 *mV*.

Examples of such characteristics are shown in Fig. 4, in comparison with the theoretical curves calculated using Eq. (39). The t_I and C values used in these calculations were chosen in such a way, as to obtain best fit between theoretical curves and experimental results. First, the t_I value was precisely determined, making use of the fact that positions of the extrema of the $V_G^0 = f(\lambda)$ curves are very sensitive functions of t_I [9]. Next, the value of C was chosen so, as to obtain the adequate vertical shift of the theoretical curve.

In addition, V_{G0} values were found and are marked in Fig. 4. This was done by taking sections of $I = f(V_G)$ characteristics, for each value of the wavelength λ and making use of the property, that for $N(0) = N(1)$ the $J = f(\Delta\phi)$ characteristic is symmetrical in respect to the $J = 0$ point, as expressed by Eqs. (57) and (58). Hence, it is concluded that each $I = f(V_G)$ characteristic which is symmetrical in respect to the $I = 0$ point corresponds with $N(0) = N(1)$. The wavelength λ used for taking such a characteristic is denoted λ_0 and the V_G^0 value for such a characteristic is equal V_{G0}.

Additional tests of selfconsistency of the applied model were made by examining the values of C (determined by the best fit between calculated curves and experimental characteristics), for MOS structures differing in values of parameters which according to Eq. (40) influence the value of C. Results of these tests were found to be quite satisfactory, as shortly described in [9].

3.2. Verification for the case of $J \neq 0$

Photocurrent versus gate voltage characteristics $I = f(V_G)$ were taken for a wide range of different Al-SiO_2-Si structures and were compared with theoretical curves calculated using formulas derived in section 2. Measurements were made on MOS capacitors with heavily doped N^+ and P^+ substrates, with a wide range of SiO_2 layer thicknesses t_I = (50 - 400) *nm* and with different thicknesses of the Al gates t_{Al} = (8 - 40) *nm*.

Comparisons between measured characteristics and calculated curves were made, as follows. From a set of $I = f(V_G)$ characteristics, taken for different wavelengths λ, the ones that are symmetric in respect to the $I = 0$ point are chosen. These are the characteristics for which electron densities at both interfaces of the dielectric are equal ($N(0) = N(1)$), as discussed in section 2 (see Eqs. (57) and (58)). Such characteristics intersect the $I = 0$ axis at $V_G = V_{GO}$. The remaining characteristics, which are not symmetric in respect to the $I = 0$ point (they are either convex or concave), intersect the $I = 0$ axis at different gate voltage values $V_G = V_G^0$, where each of the V_G^0 values corresponds with a V_I^0 value, as given by Eq. (38). Using Eq. (38), it can be shown, that for MOS structures with heavily doped substrates:

$$V_I^0 \cong V_G^0 - V_{G0} \tag{59}$$

Hence, for each of the characteristics the V_I^0 value can be determined. For a known value of V_I^0, the $N(0)/N(1)$ ratio can be found, using Eq. (31) and the entire theoretical $J = f(\Delta\phi)$ curve can be calculated, using formulas given in section 2.

Now, the calculated $J = f(\Delta\phi)$ curve has to be fitted to the experimental $j = f(V_G)$ characteristic. This is done using the normalization Eqs. (4b) and (4d). These equations contain practically only one unknown parameter m, given by the product:

$$m = \mu \cdot \theta \tag{60}$$

Thus, m becomes a fitting parameter and its value is chosen so as to obtain the best fit between the theoretical curve and the experimental characteristic.

Several examples of experimental $j = f(V_G)$ characteristics are shown in Fig. 5, in comparison with the theoretical curves, calculated and fitted to them, as described above.

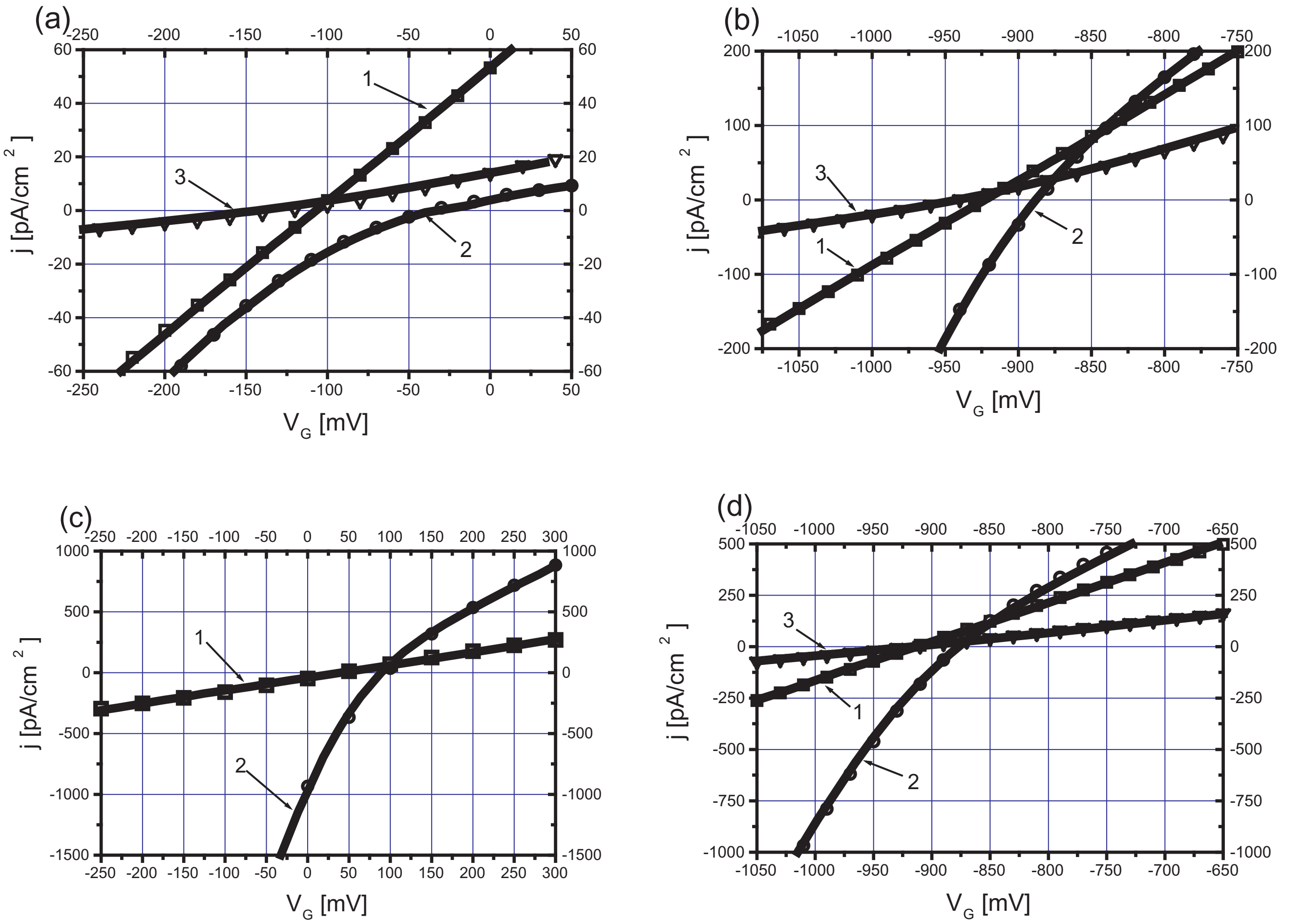

Fig. 5: Comparison of experimental $j = f(V_G)$ characteristics (squares, circles and triangles) taken on different Al-SiO_2-Si structures, illuminated with UV radiation of different wavelengths λ with corresponding theoretical curves (solid lines). (a) MOS structure with N^+ type substrate, SiO_2 layer thickness $t_I = 147$ *nm*, Al gate thickness $t_{Al} = 30$ *nm*, curve 1 : $\lambda = 244$ *nm*, $N(0)/N(1) = 1$, $m = 1.92 \times 10^{-10}$, curve 2 : $\lambda = 264$ *nm*, $N(0)/N(1) = 16.36$, $m = 2.57 \times 10^{-11}$ and curve 3 : $\lambda = 234$ *nm*, $N(0)/N(1) = 0.49$, $m = 4.28 \times 10^{-11}$. (b) P^+ substrate, $t_I = 64$ *nm*, $t_{Al} = 25$ *nm*, curve 1 : $\lambda = 246$ *nm*, $N(0)/N(1) = 1$, $m = 3.65 \times 10^{-11}$;curve 2: $\lambda = 256$ *nm*, $N(0)/N(1) = 4.29$, $m = 4.35 \times 10^{-11}$ and curve 3 : $\lambda = 236$ *nm*, $N(0)/N(1) = 0.47$, $m = 1.77 \times 10^{-11}$. (c) N^+ substrate, $t_I = 52$ *nm*, $t_{Al} = 20$ *nm*, curve 1 : $\lambda = 224$ *nm*, $N(0)/N(1) = 1$, $m = 1.77 \times 10^{-11}$ and curve 2 : $\lambda = 251$ *nm*, $N(0)/N(1) = 8.72$, $m = 5.55 \times 10^{-11}$. (d) P^+ substrate, $t_I = 155$ *nm*, $t_{Al} = 20$ *nm*, curve 1 : $\lambda = 248$ *nm*, $N(0)/N(1) = 1$, $m = 8.52 \times 10^{-10}$. Curve 2 : $\lambda = 258$ *nm*, $N(0)/N(1) = 4.13$, $m = 1.22 \times 10^{-9}$ and curve 3 : $\lambda = 238$ *nm*, $N(0)/N(1) = 0.85$, $m = 2.67 \times 10^{-10}$.

4. Discussion

The theory of photoelectric phenomena taking place when weak electric fields are present in the dielectric of the MOS system, has been developed in section 2 and has been experimentally verified, as described in section 3. The validity of this theory is strongly supported by the fact, that in spite of many simplifying assumptions made in the derivations, the agreement between the calculated curves and the experimental characteristics is quite remarkable, as demonstrated in Figs. 4 and 5.

Following aspects of these comparisons should be noticed. As mentioned in section 3, the SiO_2 layer thicknesses t_I used to calculate the $V_G^0 = f(\lambda)$ curves were the ones which assured best fit between theory and experiment in respect to the position of the extrema of the $V_G^0(\lambda)$ curves (for instance, the value of t_I(calc.) was so chosen as to assure that the minima of the experimental characteristic and of the calculated curve, shown in Fig. 4a, occur at the same wavelength λ). The so determined t_I(calc.) values turned out to be slightly (1% - 4.5%) lower than the thicknesses of the SiO_2 layer t_I(ellips.) determined by ellipsometric methods, before aluminum deposition. It was also found, that the best agreement between theory and experiment is obtained, when the thickness of the Al gate t_{Al}(calc.) used in calculation of the $V_G^0 = f(\lambda)$ curve is lower than the gate thickness t_{Al}(prof.), measured independently by profilometry (it should be borne in mind, that the shape of the $V_G^0 = f(\lambda)$ curve is much more sensitive to the changes of t_I(calc.) values, than to the changes of t_{Al}(calc.)). A more sophisticated optical model of the Al-SiO_2-Si system, based on spectroscopic ellipsometry investigations [22], confirms that indeed the effective thickness of the SiO_2 layer in a MOS structure t_I(MOS) is approximately equal to t_I(calc.) and is less than the t_I(ellips.) value (t_I(MOS) ≅ t_I(calc.) < t_I(ellips.)). This is due to the penetration of Al gate into the SiO_2 layer. Also, the same model [22], shows that the effective thickness of the Al gate layer t_{Al}(MOS) is less than t_{Al}(prof.) and is approximately equal to the t_{Al}(calc.) value (t_{Al}(MOS) ≅ t_{Al}(calc.) < t_{Al}(prof.)).

Some of the discrepancies between the calculated $V_G^0 = f(\lambda)$ curves and the corresponding experimental characteristics, which are visible in Fig. 4, result from the properties of the UV illuminating system used in this research.

Firstly, in our experiments the MOS structure was illuminated by a fairly wide wavelength band (Δλ) while calculations are made for one particular value of λ. As a result of this, the minima of the calculated $V_G^0 = f(\lambda)$ curves are often much sharper than the corresponding minima of the experimental characteristics (see e.g. Fig. 4d).

Secondly, in this research, the precision of V_G^0 determination, which is normally better than ±2 *mV*, deteriorates rapidly for wavelengths λ shorter than 215 *nm*. This manifests itself in a scatter of measurement points, as in Fig. 4d, or in significant departures of the experimental characteristics from the predicted shapes, for λ < 215 *nm*, as in Fig. 4a. Both these phenomena are caused by the rapid drop in the UV radiation output of the illuminating system used for λ < 215 *nm*.

Concerning the agreement between theory and experiment in case of the $j = f(V_G)$ characteristics shown in Fig. 5, following comment is necessary. It is the basic assumption of the theory developed in section 2, that only weak electric fields exist in the dielectric of the MOS structure. It is also assumed that the electron densities $N(0)$ and $N(1)$ are constant (which also means independent of current density J), as expressed by the boundary conditions (6). However, one may expect that for large enough photocurrents, the electron fluxes injected into the dielectric at both interfaces become insufficient to support constant values of electron densities at gate-dielectric and substrate-dielectric interfaces. This indeed is the case. When the $j = f(V_G)$ characteristics (such as the ones shown in Fig. 5) are taken in a wider range of gate voltage values, one observes, that at higher current levels, the absolute values of measured currents become lower than the ones predicted by theory. This result shows, that for large enough photocurrents, electron densities at the interfaces are no longer constant, as given by eqs. (6), but decrease with increasing current density j, as shown in more detail in [11]. For most of the Al-SiO_2-Si structures used in this research, the absolute value of the limiting electric field in the dielectric $|\mathscr{E}_{lim}|$, above which significant differences appear between the experimental results and the theory, was found to be in the range $|\mathscr{E}_{lim}| = 10^4 \div 10^5$ *V/cm*.

It is believed that the theory outlined in this article will find applications in developing a new family of photoelectric MOS structure measurement methods. Two of such applications will be mentioned here.

The first application of the results of this research is the photoelectric measurement method of the effective contact potential difference (the ϕ_{MS} factor) in the MOS system. This method, described already in [7,8] has been fundamentally improved using the results of this research and has become the most sensitive and most accurate of the existing methods of ϕ_{MS} determination. It is based on precise, photoelectric determination of the V_{GO} voltage, as discussed in sections 2 and 3. Using this method ϕ_{MS} can be determined with the accuracy of ±10 *mV*, or better. This method has already been fully verified experimentally and has been successfully applied in several investigations (see e.g. [23]).

The other application is a photoelectric method of determination of the trapping properties of the dielectric in the MOS system. It is based on measurement of the m factor, given by Eq. (60). This method which has already been shown to be sensitive to changes in trapping properties of the SiO_2 layer, subjected to plasma processing, is still being in the process of experimental verification.

5. Conclusions

A comprehensive model of photoelectric phenomena taking place in the MOS system, at low electric fields in the dielectric, has been presented. This model gives a much deeper insight into the physics of internal photoemission, allowing calculation of various photoelectric characteristics of such a system. Good agreement has been found between the calculated and experimental characteristics of a wide range of different MOS structures, which strongly supports the validity of the model. This model has been useful in developing new photoelectric MOS structure measurement methods. One of these methods, the ϕ_{MS} factor measurement method, has already been shown to be not only useful, but to be also the most accurate of the existing methods of this parameter determination.

Acknowledgments

The author is pleased to thank D. Brzezinska and Dr A. Kudla for their contribution to this research. Thanks are also due to D. Lis and Z. Sawicki for their critical remarks on the manuscript. This work is supported by the Polish State Committee for Scientific Research, under Grant No. 8T11B06116, and was presented in part at the International Conference on Modeling and Simulation of Microsystems, MSM 99, San Juan, Puerto Rico, April 19-21, 1999.

References

[1] E.H. Nicollian and J.R. Brews, "MOS Physics and Technology" (Wiley, New York, 1982).

[2] D.K. Schroder, "Semiconductor Material and Device Characterization" (Wiley, New York, 1990).

[3] R.J. Powell, "Interface barrier energy determination from voltage dependence of photoinjected currents"; J. Appl. Phys., 41, 2424-2432 (1970).

[4] C.N. Berglund and R.J. Powell, "Photoinjection into SiO_2: Electron scattering in the image force potential well"; J. Appl. Phys. 42, 573-579 (1971).

[5] R.J. Powell and C.N. Berglund, "Photoinjection studies of charge distributions in oxides of MOS structures"; J. Appl. Phys. 42, 4390-4397 (1971).

[6] H.M. Przewlocki, "On the properties of the contact potential difference in MOS structures"; in: Proceedings of the Vth International School on Physical Problems in Microelectronics. Edited by J. Kassabov, World Scientific, Singapore, pp. 62-83, 1987.

[7] H.M. Przewlocki, "Comparison of methods for ϕ_{MS} factor determination in metal-oxide-semiconductor (MOS) structures"; Electron Technol. 26, [4] 3-23 (1993).

[8] H.M. Przewlocki, "The importance, the nature and the measurement methods of the ϕ_{MS} factor in MOS structures"; Electron Technol. 27, [1] 7-42 (1994).

[9] H.M. Przewlocki, "Photoelectric phenomena in metal-insulator-semiconductor (MIS) structures at low electric fields in the insulator"; J. Appl. Phys. 78, [4] 2550-2557 (1995).

[10] H.M. Przewlocki, "A new model of photoelectric phenomena in MOS structures: Outline and applications"; in: Fundamental Aspects of Ultrathin Dielectrics on Si-based Devices, (E. Garfunkel et al Eds.) Kluwer Academic Publishers, Dordrecht, pp. 343-357, 1998.

[11] H.M. Przewlocki, "Internal photoemission characteristics of metal-insulator-semiconductor structures at low electric fields in the insulator"; J. Appl. Phys. 85, [9] 6610–6618 (1999).

[12] O.S. Heavens, "Optical Properties of Thin Solid Films"; (Butterworths, London, 1955).

[13] R.J. Powell, "Photoinjection into SiO_2: Use of optical interference to determine electron and hole contributions"; J. Appl. Phys. 40, 5093-5101 (1969).

[14] D.E. Aspnes, in: "Properties of Silicon"; edited by T.H. Ning (INSPEC 1987), EMIS Data Reviews Series No. 4.

[15] H.R. Philipp, Ibid.

[16] "Handbook of Optical Constants of Solids"; edited by E.D. Palik (Academic, Orlando FL, 1985).

[17] W. Shockley, R.C. Prim, "Space charge limited emission in semiconductors"; Phys. Rev. 90, 753-758 (1953).

[18] G.H. Suits, "Exact current-voltage relation for the metal-insulator-metal junction with a simple model for trapping of charge carriers"; J. Appl. Phys. 28, 454-458 (1957).

[19] E.I. Adirovich, "Elektricheskie polia i toki v dielektrikakh"; (in Russian), Electric fields and currents in dielectrics, Solid State Physics, 2, 1410-1422 (1960).

[20] M. Abramovitz, I.A. Stegun, "Handbook of Mathematical Functions" (Dover, New York, 1965).

[21] W.J. Thompson, "Atlas for Computing Mathematical Functions" (Wiley, New York, 1997).

[22] A. Kudla, D. Brzezinska, J. Katcki, T. Wagner, "Determination of optical parameters of the MOS structure for use in photoelectric measurements"; Electron Technol. 32, 391-396 (1999).

[23] H.M. Przewlocki, H.Z. Massoud, "Photoelectric investigation of the processing dependence of the effective contact potential difference in MOS devices"; US-Poland MCS Fund II Project MP/NIST-94-200 Final Report (Warsaw, Poland, Durham N.C., USA 1998).

Received in Cambridge, MA, USA, 2nd September 1999

Paper 1/02774